Transactions of the Korean Nuclear Society Autumn Meeting
Gyeongju, Korea, October 29-30, 2015

CFD Investigation for Flow Blockage Accident in a Lower Plenum

J. Yoo*, J. H. Jeong, W. P Chang, K. S Ha
Korea Atomic Energy Research Institute
P.O.Box 105, Yuseong, Daejeon, 305-600, Korea
**Corresponding author: yoojin@kaeri.re.kr*

1. Introduction

A flow blockage accident occurred at the Fermi plant in 1966. A piece of zirconium liner that had broken loose moved into the core inlet region, creating a flow blockage that caused fuel damage. Since the Fermi incident, the inlet nozzles for the fuel assemblies include multiple coolant inlet passages so that complete external blockages would not be possible. However, NRC assigned the blockage event as the 7th bounding event (BE-7) for the PRISM design because of likelihood for a fabrication error[1]. Large Partial Inlet flow blockage is involved as a BE (Bounding Event) in PGSFR[2]. There are no known sources for objects of this nature in the inlet plenum but one could postulate that a large object might be gotten down to lower plenum[3]. It is possible to block the entrance of nozzle at receptacle which has 6 nozzles located just below the orifice plates. Then it can cause the flow reduction that flows into a fuel assembly and affect cladding integrity.

Therefore, it is necessary to investigate how much flow rate would be decreased by large partial inlet blockage accident. The objective of the present study is to predict the flow reduction of hottest assembly as well as flow features in a lower plenum when orifice nozzle under hottest assembly is blocked by large objects.

2. Physical geometry and numerical models

2.1 Geometry and Momentum Loss Model

Figure 1 show PGSFR core configuration. It is consisted of 112 inner/outer fuel assemblies including hottest assemblies, 90 reflector assemblies, 102 shield assemblies, 9 control rod assemblies. As the power distribution in the reactor is not uniform, flow through each assembly has to be allocated such that temperature at the outlet of the assembly is nearly uniform. However, it is cumbersome to allocate flow for each assembly and hence assemblies having similar powers are grouped together and are assigned the same flow. Assembly for PGSFR is divided into a number of 12 flow groups shown in Table 1. The flow rate is controlled by orifice plate inside receptacle to allocate assemblies adequately. In this case momentum loss model with the resistance coefficient is used in defined subdomain instead of modeling all sub-assemblies in core. When modeling porous momentum losses, a momentum loss due to an obstruction in the flow direction, the isotropic and directional loss models are useful. When using the isotropic loss model it simply adds a source term to the momentum equation follows.

$$S_{Mi} = -\frac{\mu}{k_{perm}} u_i - k_{loss} \frac{1}{2} \rho u_i^2 \qquad (1)$$

Where S_{Mi} is a momentum source terms, k_{perm} is the permeability coefficient (for the viscous loss), and k_{loss} is the resistance loss coefficient (for the inertial loss). The first term represents viscous losses, whereas the second term represents inertial losses.

For resistance loss coefficient, the correlation is expressed as [4]

$$k_{loss} = C \,\mathrm{Re}^{n1} \beta^{n2} \left(\frac{D_e}{D_2}\right)^{n3} \left(\frac{l_e}{D_2}\right)^{n4} \left(\frac{b}{h}\right)^{n5} \qquad (2)$$

Where u_i is the mean flow velocity at the side-orifice which is calculated from upstream mass flux using mass conservation and D_e is the equivalent diameter of the side-orifice, β is area ratio(A_i =cross sectional area of side orifice, A_2 =area of downstream section), l_e is leading edge, and D_e / D_2 is ratio of equivalent diameter of side-orifice to downstream diameter, l_e / D_2 is ratio of leading edge length of side-orifice to downstream diameter, b / h is ratio of average width to height of side-orifice, n_1, n_2, n_3, n_4, n_5 is constant value depending on the reynold number. The geometry of side-orifice in a lower plenum is shown in Figure 2.

The resistance loss coefficient is caused primarily by the turbulence and vortex motion created by the enlargement of the stream after it passes orifice nozzle[5, 6].

In this study, flow rate of hottest assembly was predicted in accordance with a number of side-orifice by applying to k_{loss} which is known value from the equation (2) by postulating the large partial inlet flow blockage.

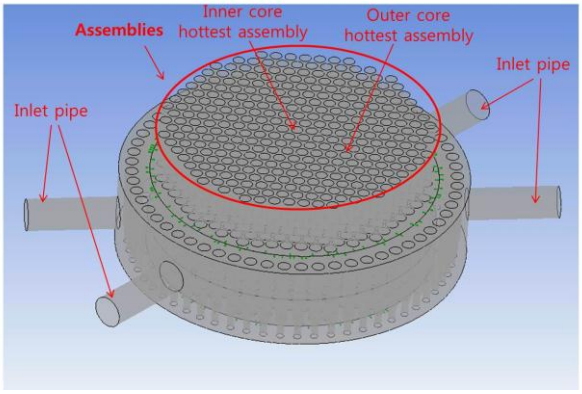

Figure 1 Core Configuration in PGSFR

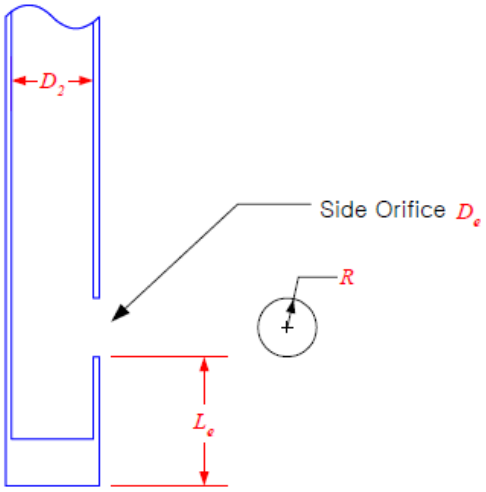

Figure 2 Geometry of side-orifice in a lower plenum

Table 1. Flow Group and Flow Rate for each Group

Flow Group No.	150 MWe PGSFR			
	Ass. Type	# of Ass.	Ass. Rate [kg/s]	Group Rate [kg/s] (%)
1	Inner	10	23.57	235.7 (11.84)
2	Inner	12	22.22	266.6 (13.40)
3	Inner	12	21.09	253.0 (12.72)
4	Inner	18	19.17	345.1 (17.34)
5	Outer	12	15.82	189.8 (9.54)
6	Outer	12	15.16	181.9 (9.14)
7	Outer	6	13.79	82.72 (4.16)
8	Outer	18	12.34	222.1 (11.16)
9	Outer	12	11.08	132.9 (6.68)
10	Control	9	1.65	14.85 (0.75)
11	Reflector	90	0.173	15.55 (0.78)
12	Shield	102	0.0953	9.719 (0.49)
Total	-	313	-	1950.0 (98.0)

2.2 Accident Scenarios

For a large partial inlet blockage, it was conservatively assumed that, a hypothetical large object would block the entrance of orifice slotted under hottest assemblies which has 6 nozzles shown in Figure 3. In the event that nozzle at orifice is blocked by a large object, the primary coolant would not flow into the inner/outer hot assemblies which represent the lowest flow among the various assemblies with the maximum power. Assuming up to 5 nozzles is blocked by a large object, the CFD analyses were performed.

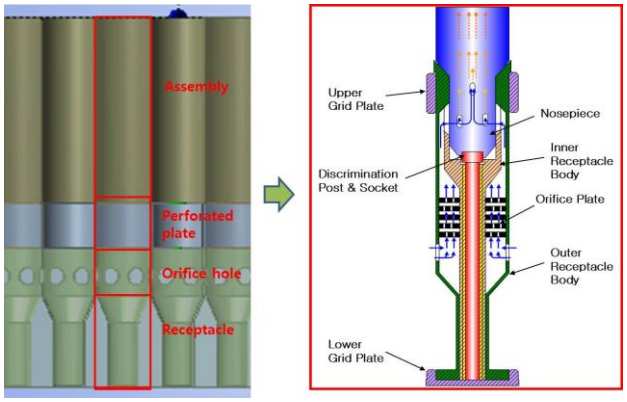

Figure 3 Details of side orifice in PGSFR

2.3 turbulence models

In this study, the flow patterns in a lower plenum are obtained by solving the steady state, three-dimensional Reynolds-averaged Navier-Stokes equations for incompressible flow. Because the heat transfer is not concerned in the present study, the energy conservation equation is not included.

A realizable k-ε turbulence model developed by Shih et al. (1994) and utilizing a high y+ wall treatment is used[7]. This turbulence model contains transport equations for the turbulent kinetic energy k and turbulence dissipation rate ε. This turbulence model was chosen because it generally provides better predictions than the standard k-ε when the flow involves rotation, recirculation, and separation, all of which would be expected in the lower plenum region.

Figure 4 and Table 2 show comparison between the designed flow and CFD values in case of no-blockage at orifice nozzle. Considering the complexity of the lower plenum geometry due to receptacle structures, the agreement is good. The commercial CFD code, CFX 14.5 is employed to solve the Reynolds-averaged Navier-Stokes equations for incompressible flow with the Realizable k-ε turbulence model, and to post-process the results.

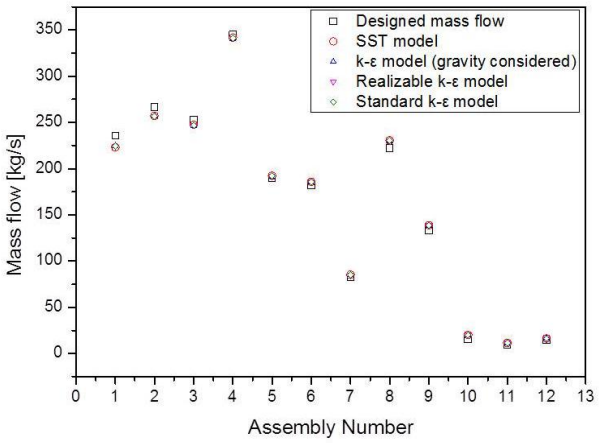

Figure 4 Mass flow comparison between designed and CFD values

Table 2. Deviation between designed and CFD values

Assembly group	NAME OF ASSEMBLY	Designed mass flow	CFD mass flow	Deviation between designed and analysis value
1	Inner	235.7	223.3	4.877387
2	Inner	266.6	257.0	3.692048
3	Inner	253	247.4	2.394466
4	Inner	345.1	341.7	1.171544
5	Outer	189.8	192.4	-1.26923
6	Outer	181.9	185.8	-2.06377
7	Outer	82.72	85.2	-3.06214
8	Outer	222.1	230.5	-3.76092
9	Outer	132.9	138.8	-4.47329
10	reflector	15.55	20.1	-29.5177
11	shield	9.719	11.5	-18.1912
12	control	14.85	16.4	-10.3838

2.4 Boundary conditions

Table 3 shows the boundary condition in a lower plenum. In this study, it is modeled only for fluid region for reducing the computational time. The inlet and outlet boundary conditions are imposed as mass flow inlet (1950 kg/s) and static pressure outlet, which are as the normal operating condition, respectively. No-slip walls are applied on the surfaces of model. The sodium properties are imposed as a function of temperature for this simulation. Table 4 illustrated physical properties of Sodium at normal operation

Table 3 Boundary condition

Variable	Values
Mass flow rate inlet (kg/s)	1950
Static Pressure outlet (Pa)	0
No-slip wall	-

Table 4 Physical properties of Sodium

Variable	Values
Density (Kg/m3)	864.1
Dynamic viscosity (Pa s)	0.0002808
Specific heat (J/kg K)	1286

2.5 Grid Dependency Study

In numerical analysis, the mesh plays an important role for the calculation of simulation and is thus necessary to find an optimal balance between the number of cells and the hardware requirements for computing, which brings with it the number of cells. Therefore three cases have been taken with different mesh size, which is tabulated in Table 5. Table 5 shows three cases depending on size of grid used for grid dependency study. Mesh refinement has been performed close to the wall boundaries.

Table 5. Number of elements for different mesh type

Type of mesh	Case #1	Case# 2	Case #3
Tetra	8159323	9959323	11161560
Prisms	1389539	1789539	8491755
Hexa	504780	954780	5238457
Elements	3102879	8182899	24891772

Predicted flow rate at outlet (Table 5) for three different mesh sizes don't show very great change in result with a difference of 1%. Further refinement of the mesh was attempted, but the simulation results were hardly changed.

3. Computational Results

The steady state was simulated. The convergence criteria were set to 1.0E-04 for RMS residuals (mass, momentum). Figure 5 illustrates top view of lower plenum. The calculated results using realizable k-ε turbulence model were post-processed by cross sectional A-A' and B-B' view.

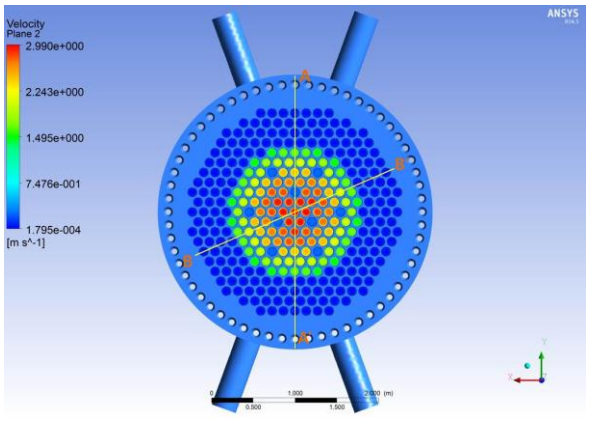

Figure 5 Top view of lower plenum

3.1 Case without blockage at orifice nozzle

Figure 6 shows velocity distribution on the cross sectional plane perpendicular to Z-direction. It is observed that flow coming into lower plenum is distributed to the individual assembly. The flow right after entering into the lower plenum through inlet pipe shows imperfect flow mixing. But it is thought to create sufficient mixing as flow is distributed into the assembly. It shows that velocity profile in a lower plenum is assumed that results are qualitatively reasonable.

Figure 7 shows velocity distribution on B-B' cross sectional plane without blockage at orifice (0 % blockage). It is clearly understood that velocity distribution through each assembly looks symmetric at the outlet of assembly because flow is divided into a number of 12 flow groups as shown in Table 1. Velocity distribution in accordance with the different flow groups is obviously affected by a momentum loss modeling (for details see equation 2).

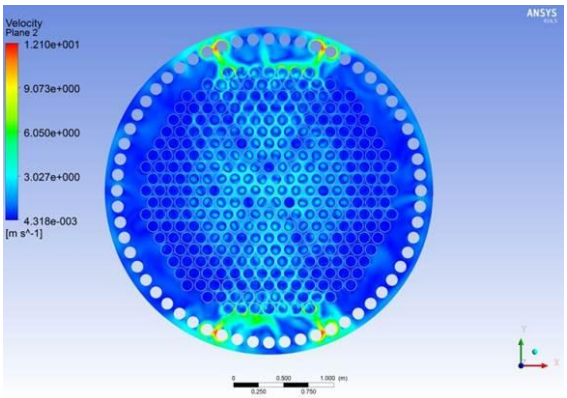

(a) Z =0.2 m

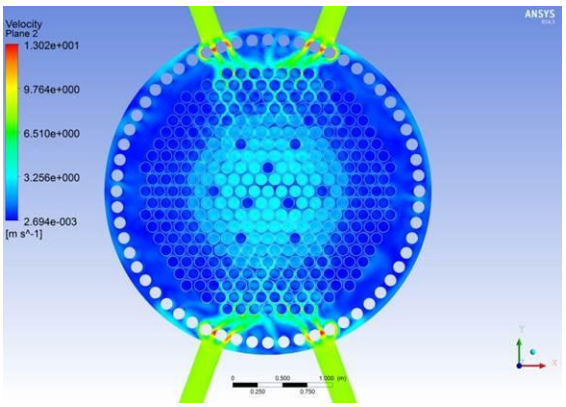

(b) Z =0.3 m

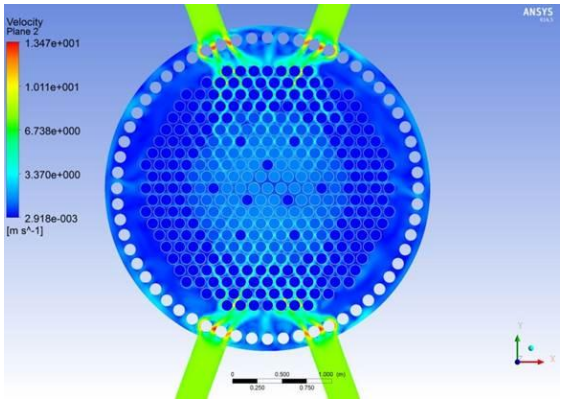

(c) Z =0.4 m

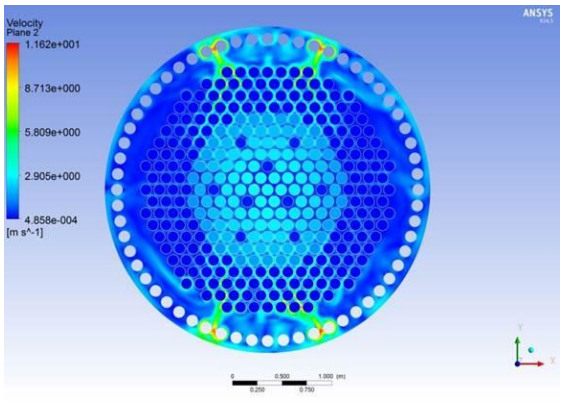

(d) Z =0.6 m

Figure 6 Velocity distribution on the cross sectional plane perpendicular to Z-direction

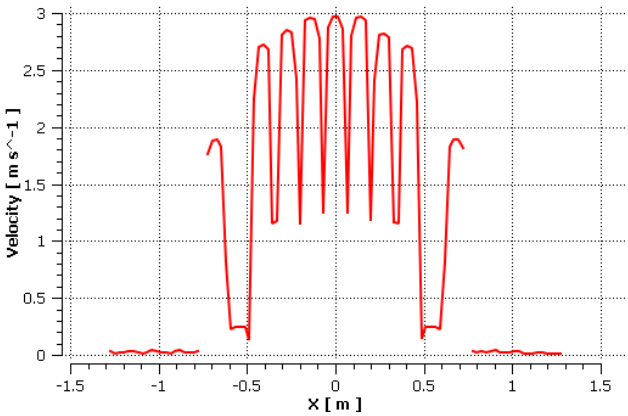

Figure 7 Velocity distribution on B-B' cross sectional plane without blockage at orifice (0 % blockage)

3.2 Case with blockage at orifice nozzle

Figure 8 shows comparison of velocity distribution on the B-B' cross sectional plane as a function of number of blockage. It can be clearly seen that the velocity distribution varies as a number of blocked nozzle at orifice increase. The velocity variation originating in hottest assembly substantiates this finding shown in Figure 9.

Figure 10 shows comparison of velocity vector between no-blockage and 5-orifice nozzle blockage. In

the no-blockage case, the velocity vector around the side orifice nozzle has symmetry because flow is uniformly distributed through 6-side orifice nozzle. The velocity of flow right after passing through orifice nozzle increases very rapidly which is estimated as maximum 7.5 m/s and pressure drops abruptly. This is the conversion of potential energy to kinetic energy in compliance with the Bernoulli's theorem. When the fluid leaves the vena contracta as shown in Figure 10, its velocity decreases and its pressure increases as kinetic energy is converted back into potential energy.

For 5-orifce nozzle blockage cases, recirculation around the side orifice nozzle was found, which is asymmetric and complex. This means that reduced flow area had a more influence on friction loss by viscosity and it occurred more flow resistance compared to no-blockage case. The maximum velocity for the 5-orifice nozzle blockage case was estimated as 13 m/s

Figure 11 shows flow rate variations as a function of number of blocked nozzle in a hottest assembly. The more blockage area at orifice increases, the more flow rate of the hottest assembly decreases. The maximum reduced flow of hottest assembly was predicted to be about 9.32 kg/s. In the case of 5-orifice nozzle blockage which corresponds to the blockage area of 83.3%, the maximum reduced flow is about 58 % compared to no-blockage case. Considering that the flow rate of no-blockage case is 22.3 kg/s, it is substantial flow rate reduction.

Figure 12 shows flow rate variations of individual assembly group as a function of number of blocked nozzle in a hottest assembly. It can be clearly seen that flow rate of 1 group including hottest assembly was decreased as flow blockage area is increased. It means that flow rate entering into hottest assembly is reduced whereas flow rate flowing into other assembly is increased.

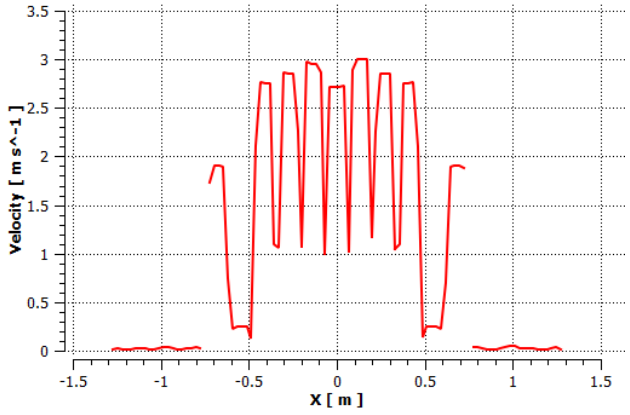

(a) 2-blockage at orifice (33.3 % blockage)

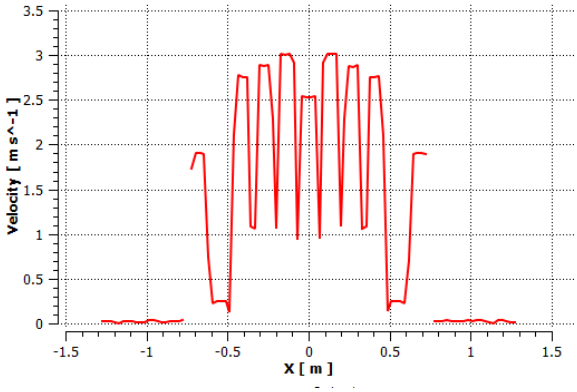

(b) 3-blockage at orifice (50 % area)

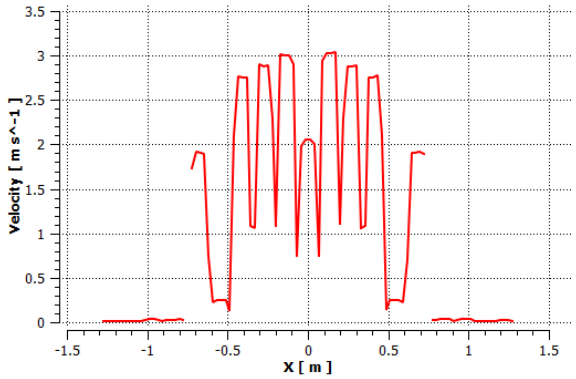

(c) 4-blockage at orifice (66.7 % blockage)

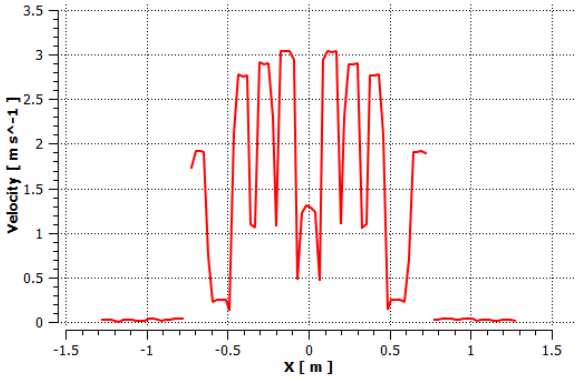

(d) 5-blockage at orifice (83.3 % blockage)

Figure 8 Comparison of velocity distribution on the B-B' cross sectional plane as a function of number of blockage

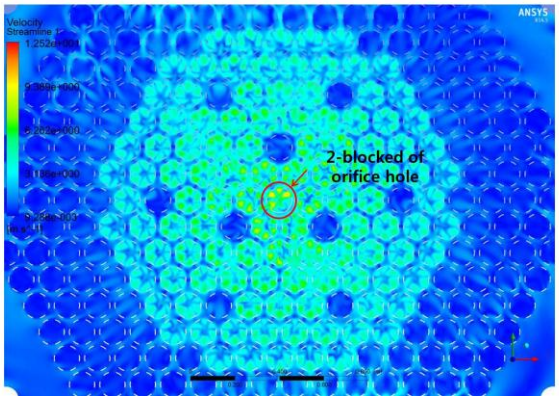

(a) 2-blockage at orifice nozzle

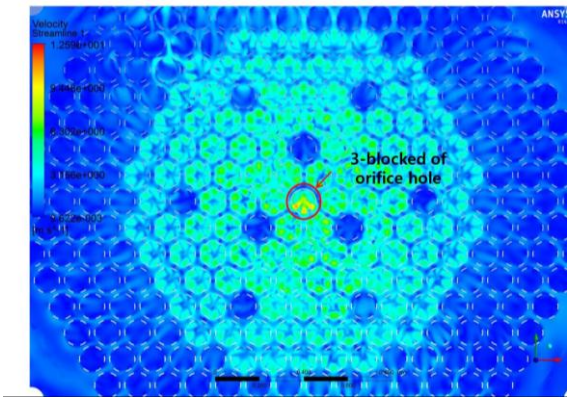

(b) 3-blockage at orifice nozzle

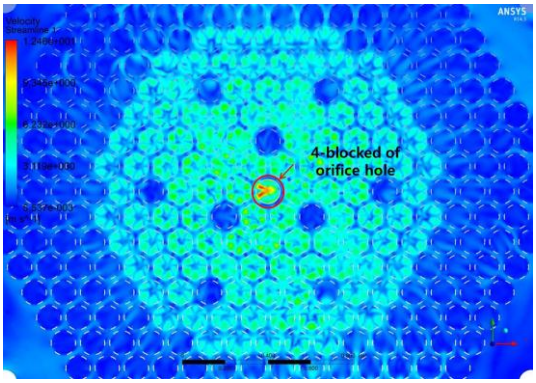

(c) 4-blockage at orifice nozzle

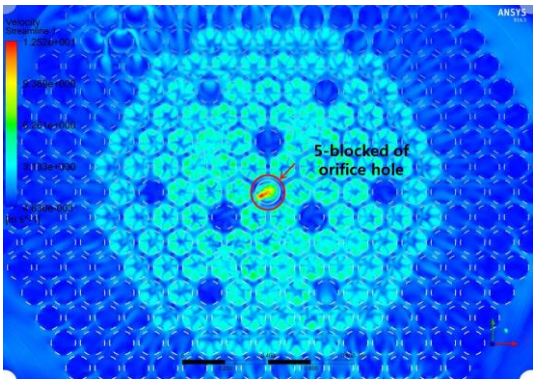

(d) 5-blockage at orifice nozzle

Figure 9 Comparison of velocity contours at Z=0.25m

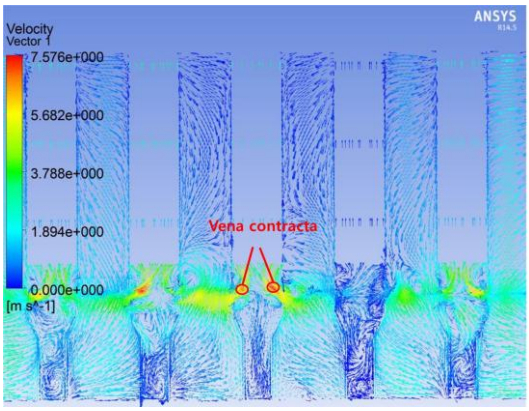

(a) no-blockage

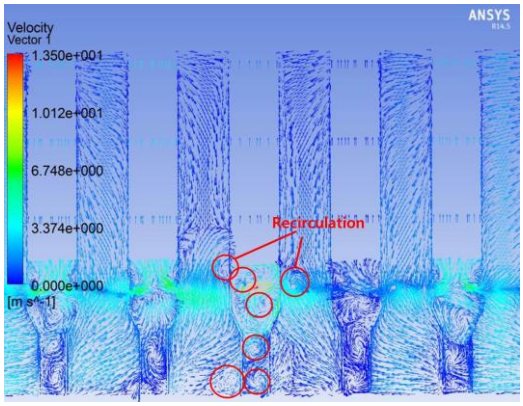

(b) 5-blockage

Figure 10 Comparison of velocity vector between No-blockage and 5-orifice nozzle blockage

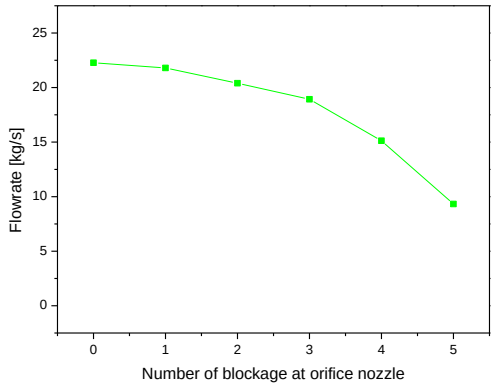

Figure 11 Flow rate variations as a function of number of blocked nozzle in a hottest assembly

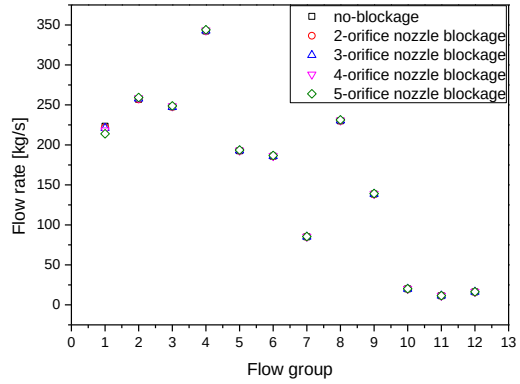

Figure 12 Flow rate variations of individual assembly group as a function of number of blocked nozzle in a hottest assembly

4. Conclusions

A CFD analysis by fully resolved RANS simulations has been carried out to predict effects of flow blockage at side orifice as well as flow feature in a lower plenum.

In the no-blockage case, the velocity vector around the side orifice nozzle has symmetry because flow is

uniformly distributed through 6-side orifice nozzle. The velocity of flow right after passing through orifice nozzle increases very rapidly which is estimated as maximum 7.5 m/s and pressure drops abruptly. This is the conversion of potential energy to kinetic energy in compliance with the Bernoulli's theorem. For 5-orifce nozzle blockage cases, recirculation around the side orifice nozzle was found, which is asymmetric and complex. This means that reduced flow area had a more influence on friction loss by viscosity and it occurred more flow resistance compared to no-blockage case. The maximum velocity for the 5-orifice nozzle blockage case was estimated as 13 m/s

The more blockage area at orifice increases, the more flow rate of the hottest assembly decreases. The maximum reduced flow of hottest assembly was predicted to be about 9.32 kg/s. In the case of 5-orifice nozzle blockage which corresponds to the blockage area of 83.3%, the maximum reduced flow is about 58 % compared to no-blockage case. Considering that the flow rate of no-blockage case is 22.3 kg/s, it is substantial flow rate reduction.

REFERENCES

[1] U. S. NRC, "Preapplication Safety Evaluation Report for the Power Reactor Innovative Small Module (PRISM) Liquid-Metal Reactor," NUREG-1368, 1994.
[2] Kwi-Seok Ha, "Safety Analysis Methodology for Design Basis and Transient Accident in SFR", SFR-900-DS-474-001, April, 2014.
[3] Clinch River Breeder Reactor Project, "Preliminary Safety Analysis Report," Volume 9, June, 1975.
[4] J. R. Park et al., "A Study on the Flow Redistribution in Lower Plenum of LMR during Transition Flow, KAERI/CM-103/96, 1996.
[5] Moon. Hynu. Chun et al., "An Experimental Investigation of the Effects of the sudden Contraction on Single- and Two-Phase Pressure Drop," Journal of the Korean Nuclear Society, Volume 21, June, 1989
[6] Khanzhonkov V. I. and Davydonko N. I., "Resistance of Side Orifices of the Thermal Section of a Pipeline," Prom. Arodin., no.15, 38-46, Oborongiz, Moscow, 1959.
[7]Shih, T., Liou, W., Shabbir, A., Yang, Z., and Zhu, J., "A new k-epsilon eddy viscosity model for high Reynolds number turbulent flows," NASA STI/Recon Technical Report N,95p.11442, 1994.
[8] H. Farajollahi et al., "CFD-Calculation of Fluid Flow in a Pressurized Water Reactor," Journal of Sciences, Islamic Republic of Iran, Summer, 2008
[9] Thomas Hohne et al., "CFD Simulation of Thermal-Hydraulic Benchmark V1000CT-2 Using Ansys CFX," Science and Technology of Nuclear Installation, Hindawi Publishing Corporation, January, 2009
[10] R.W. Lyczkowski., "Analysis of A PWR Downcomer And Lower Plenum Under Asymmetric Loop Flow Conditions," American Nuclear Society, Boston, June, 1985